atmosphere

MDPI

Article

ARIMA Analysis of PM Concentrations during the COVID-19 Isolation in a High-Altitude Latin American Megacity

David Santiago Hernández-Medina, Carlos Alfonso Zafra-Mejía * and Hugo Alexander Rondón-Quintana

Grupo de Investigación en Ingeniería Ambiental-GIIAUD, Facultad del Medio Ambiente y Recursos Naturales, Universidad Distrital Francisco José de Caldas, Bogotá E-110321, Colombia; dshernandezm@udistrital.edu.co (D.S.H.-M.); harondonq@udistrital.edu.co (H.A.R.-Q.)

* Correspondence: czafra@udistrital.edu.co

Abstract: The COVID-19 pandemic precipitated a unique period of social isolation, presenting an unprecedented opportunity to scrutinize the influence of human activities on urban air quality. This study employs ARIMA models to explore the impact of COVID-19 isolation measures on the PM_{10} and $PM_{2.5}$ concentrations in a high-altitude Latin American megacity (Bogota, Colombia). Three isolation scenarios were examined: strict (5 months), sectorized (1 months), and flexible (2 months). Our findings indicate that strict isolation measures exert a more pronounced effect on the short-term simulated concentrations of PM_{10} and $PM_{2.5}$ (PM_{10}: −47.3%; $PM_{2.5}$: −54%) compared to the long-term effects (PM10: −29.4%; $PM_{2.5}$: −28.3%). The ARIMA models suggest that strict isolation measures tend to diminish the persistence of the PM_{10} and $PM_{2.5}$ concentrations over time, both in the short and long term. In the short term, strict isolation measures appear to augment the variation in the PM_{10} and $PM_{2.5}$ concentrations, with a more substantial increase observed for $PM_{2.5}$. Conversely, in the long term, these measures seem to reduce the variations in the PM concentrations, indicating a more stable behavior that is less susceptible to abrupt peaks. The differences in the reduction in the PM_{10} and $PM_{2.5}$ concentrations between the strict and flexible isolation scenarios were 23.8% and 12.8%, respectively. This research provides valuable insights into the potential for strategic isolation measures to improve the air quality in urban environments.

Keywords: ARIMA; COVID-19; particulate matter; lockdown; air quality

Citation: Hernández-Medina, D.S.; Zafra-Mejía, C.A.; Rondón-Quintana, H.A. ARIMA Analysis of PM Concentrations during the COVID-19 Isolation in a High-Altitude Latin American Megacity. *Atmosphere* **2024**, *15*, 683. https://doi.org/10.3390/atmos15060683

Academic Editors: Zhaobin Sun, Jun Yang and Ling Han

Received: 29 April 2024
Revised: 27 May 2024
Accepted: 29 May 2024
Published: 2 June 2024

1. Introduction

Air pollution, a global concern requiring urgent attention, imposes a significant economic strain on public health systems [1]. In 2019, it was responsible for an estimated 4.2 million premature deaths, with 38% due to ischemic heart disease, 20% to heart attacks, and 43% to chronic obstructive pulmonary disease [2]. Particulate Matter (PM), a key air pollutant, has a significant impact on public health. PM, comprising small-diameter particles of inorganic and organic substances, originates from coal combustion, thermal power plants, and industrial activities [3]. The severe effects of PM on the pulmonary and cardiac systems persist even at low exposure levels, particularly for particles with diameters $\leq$ 10 µm (PM_{10}) and $\leq$2.5 µm ($PM_{2.5}$) [4]. The smallest particles ($PM_{2.5}$) evidence the greatest problems, because they can penetrate deep into the lungs and even reach the bloodstream. This phenomenon increases their toxicity, because they can cause or worsen respiratory and cardiovascular problems [5]. This issue is exacerbated in low- and middle-income countries, where a large segment of the population is exposed to PM. As a result, there is a significant economic burden due to the increased mortality and morbidity rates arising from cardiovascular and respiratory diseases [1]. The main sources of PM_{10} and $PM_{2.5}$ in urban environments are primary combustion, such as vehicle emissions, coal combustion, biomass burning, secondary aerosol formation, industrial emissions, and dust sources [6].

The COVID-19 pandemic precipitated an acute respiratory disease, prompting the global implementation of social isolation measures to curb the spread of this novel biological agent [7]. These unprecedented social restrictions profoundly influenced global economic dynamics, social interactions, and urban environments [4]. This period of social isolation provided a unique opportunity to study the impact of human activities on urban air quality. The behavior of pollution emission sources underwent significant changes during the pandemic. Mobile sources (e.g., vehicles) [8,9], stationary sources (e.g., factories) [10,11], and fugitive sources (e.g., construction sites) [12,13] all responded to the isolation measures imposed by COVID-19. Consequently, the urban concentrations of PM_{10} and $PM_{2.5}$ exhibited notable reductions [14,15]. These reductions were attributed to measures such as limiting vehicular traffic, restricting public transportation mobility, and curbing non-essential industrial production [16]. However, not all cities experienced uniform air quality changes. Some reported increases in the PM_{10} and $PM_{2.5}$ concentrations [17,18]. The factors contributing to these increases included heightened household utility usage (e.g., natural gas and electricity) and the economic reactivation following the isolation period [19]. For instance, during the strict lockdowns in Indian cities like Chennai, New Delhi, and Kolkata, the PM_{10} and $PM_{2.5}$ concentrations decreased by approximately 65% and 73%, respectively [20]. In contrast, Saudi Arabia witnessed PM concentration increases, likely due to regional phenomena like sandstorms and urban dust resuspension [17]. In the megacity of Bogota, Colombia, strict isolation measures led to a substantial reduction in PM_{10}, NO_2, and $PM_{2.5}$ concentrations—approximately 39%, 63%, and 34%, respectively [7]. While meteorological conditions also played a role, historical observations during this period suggest that changes in human behavior were the primary drivers of the improved air quality [7,21].

The fluctuations in the PM concentrations within our study megacity during the COVID-19 isolation provide a unique lens through which to examine this air pollutant's behavior under conditions of reduced anthropogenic activity. This analysis holds particular significance given PM's central role in the megacity's air quality monitoring and control efforts [22]. PM's relevance in our megacity stems from its frequent exceedances of the permissible limit values for both PM_{10} and $PM_{2.5}$. While these elevated concentrations are often associated with human activities, they may also result from the unfavorable meteorological conditions that hinder atmospheric dispersion. Factors such as persistent thermal inversions, reduced precipitation, and wind patterns conducive to the influx of external pollutants all contribute to these exceedances [23,24]. Moreover, regional events—such as biomass burning in nearby crops—can introduce external air pollutants [25]. Therefore, our investigation sheds light on the dynamics of PM in a megacity during a unique period of reduced human activity, emphasizing the need for comprehensive air quality management strategies. While there is some literature on air quality changes during COVID-19, few studies have focused on high-altitude urban environments where the atmospheric dynamics can differ significantly.

During efforts to prevent and mitigate air pollution events, governmental entities and research centers have increasingly turned to modeling techniques to generate early warnings of air quality deterioration [26]. These models serve as valuable tools for air pollution control and management [27]. Simulation models such as Weather Research and Forecasting (WRF) or the WRF-CMAQ require a substantial amount of air quality data and meteorological information to achieve accurate predictions [26,28]. To address this need, researchers have explored the individual modeling of air pollutants using time series analysis—a statistical approach based on continuous observations of a variable of interest over a specific time interval [29,30]. Among the time series analysis techniques, Autoregressive, Integrated, and Moving Average (ARIMA) models play a prominent role. ARIMA models allow for the study of air pollutants individually and over time by analyzing correlations within the data series itself [31]. The ARIMA model comprises three key components: (1) an Autoregressive (AR) component, which accounts for the regressors of the time series and reflects the model's memory [32,33]; (2) an Integrated (I)

component, which is associated with the number of differences needed to make the time series stationary (i.e., independent of time) [33]; and (3) a Moving Average (MA) component, which addresses random shocks and inherent variability within the time series [33]. The ARIMA structure facilitates the simulation of parameter behavior in the presence of external variables by capturing linear trends within the time series [34]. By leveraging these models, researchers can enhance our understanding of air pollutant dynamics and contribute to effective pollution management strategies.

The application of ARIMA models in analyzing urban PM concentrations has garnered attention across several studies [35,36]. Notably, the optimal ARIMA simulations of the PM concentrations were observed at an hourly timescale, during short time intervals, and in the urban areas characterized by low pollutant persistence (where the autoregressive [AR] term was less than 4) [26,37]. Sensitivity analyses revealed that the ARIMA models performed well when dealing with a PM concentration series exhibiting substantial temporal variability [38]. This variability in the PM concentrations was closely linked to unfavorable meteorological conditions for air pollutant dispersion [31] and regional particle transport phenomena [39]. Megacities provided an ideal testing ground, where persistent PM_{10} (with AR terms exceeding 8) and variable PM_{10} (with moving average [MA] terms exceeding 8) were observed in the areas dominated by impervious surfaces [40]. Furthermore, the ARIMA models were pitted against other modeling approaches (such as Long Short-Term Memory [LSTM], Random Forest Regression [RFR], and Support Vector Regression [SVR]) to explore the concentration behavior of PM during the COVID-19 isolation. The ARIMA models demonstrated a satisfactory performance within this context [41]. Moreover, the historical $PM_{2.5}$ concentration series were compared with those observed during the COVID-19 isolation. The latter exhibited higher persistence and variability, underscoring the unique impact of pandemic-related behavioral changes on urban air quality [4].

The objective of this work is to investigate by means of ARIMA models the effect of COVID-19 isolation measurements on the PM_{10} and $PM_{2.5}$ concentrations in Bogota, Colombia—a megacity located at a high altitude. Leveraging the ARIMA models, we explore the following three distinct scenarios for the PM concentrations: (1) the historical series, examining pre-pandemic data; (2) pre-isolation, assessing the PM concentrations before the initial isolation measures; and (3) during isolation, analyzing the impact of various social isolation strategies (strict, sectorized, and flexible) implemented by the city administration. Our study holds practical significance in the field of urban pollution for the following reasons. (1) The Evaluation of ARIMA Models: We assess the utility of ARIMA models in studying urban air quality interventions. These models allow us to dissect the temporal dynamics of the PM concentrations. (2) A High-Altitude Context: Bogota's unique high-altitude conditions introduce additional complexities. We investigate how COVID-19 isolation influenced the PM levels in this challenging environment. (3) Temporal Structure Analysis: By examining different types of social isolation measures, we gain insights into the temporal behavior captured by our ARIMA models. Lastly, this research contributes to our understanding of the pandemic-induced changes in air quality and informs effective pollution management strategies.

2. Materials and Methods

2.1. Study Site Description

The megacity under investigation is situated in Colombia (South America, 4°35′53″ N–74°4′33″ W). Bogota, the capital of Colombia, is positioned at an average elevation of 2640 masl and is recognized as one of the most densely populated megacities in Latin America, with a density of 272 inhabitants/Ha. This density surpasses the Latin American average by a factor of 2.5 [42]. Owing to its proximity to the equator, this megacity does not experience distinct seasons and maintains an average annual temperature ranging between 14 and 15 °C. Its elevated location results in hourly temperature fluctuations reaching up to 17.9 °C within a single day. The annual precipita-

tion pattern reveals two periods of increased precipitation: March–May and September–November [43]. For the purpose of air quality monitoring, four stations were selected (RMCAB, http://rmcab.ambientebogota.gov.co/home/map (accessed on 1 February 2022). These stations are identified as follows (Figure 1): Centro de Alto Rendimiento—CAR, Kennedy—KEN, Las Ferias—LAF, and Tunal—TUN. The selection criteria for these stations included comprehensive coverage of the megacity and data availability exceeding 90% for the PM_{10} and $PM_{2.5}$ concentrations. The characteristics of these monitoring stations are detailed in Table 1.

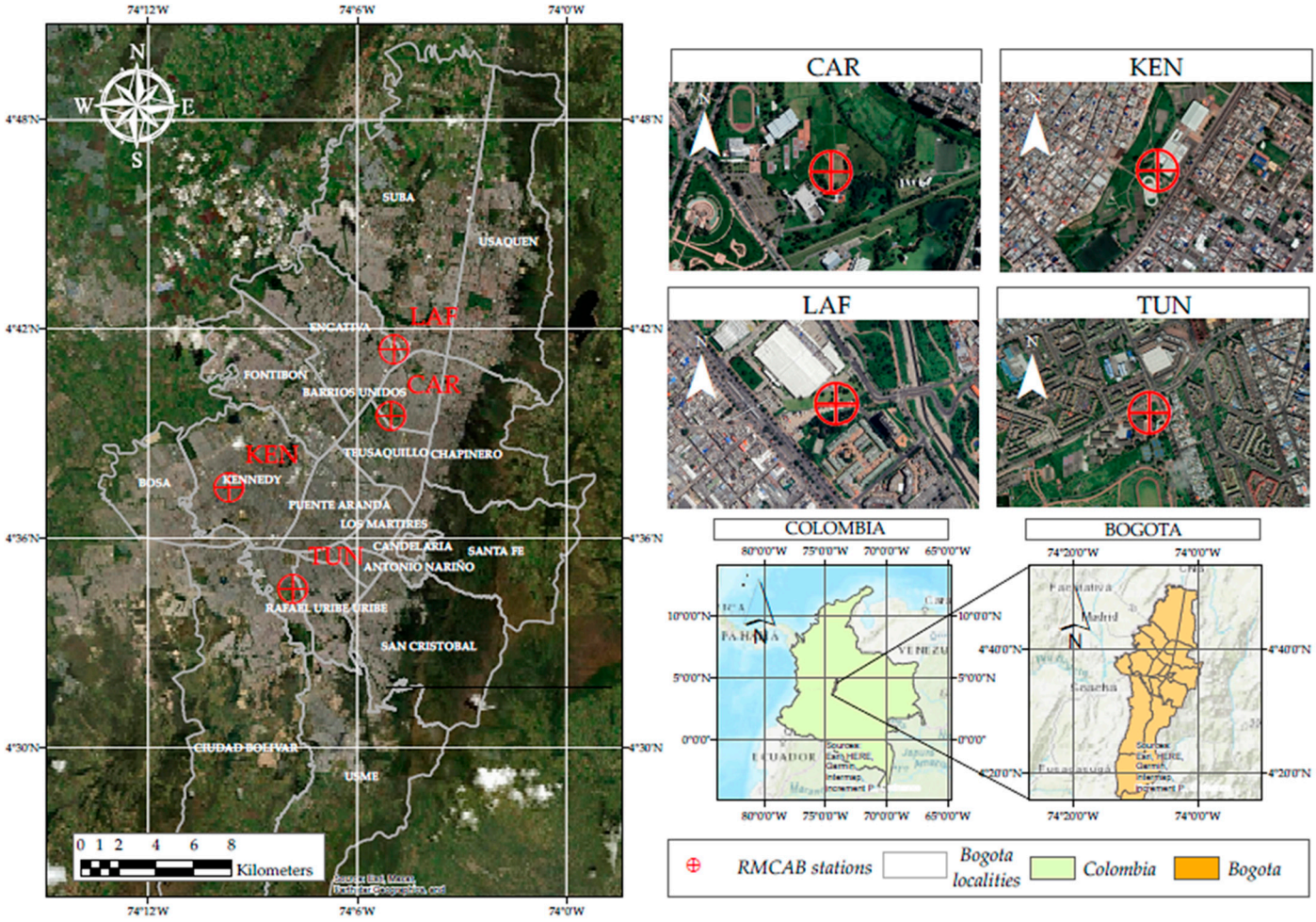

Figure 1. Location of monitoring stations in the megacity of study (Bogota, Colombia).

Table 1. Characteristics of selected air quality monitoring stations.

Characteristic	Monitoring Stations			
	CAR	**KEN**	**LAF**	**TUN**
Coordinates	4°39′30.48″ N	4°37′30.18″ N	4°41′26.52″ N	4°34′34.41″ N
	74°5′2.28″ W	74°9′40.80″ W	74°4′56.94″ W	74°7′51.44″ W
Atmospheric pollutants	PM_{10}, $PM_{2.5}$	PM_{10}, $PM_{2.5}$	PM_{10}, $PM_{2.5}$	PM_{10}, $PM_{2.5}$
Meteorological variables	VV, DV, T, Pr, HR	VV, DV, T, Pr, RS, HR, Ps	VV, DV, T, Pr, HR, Ps	VV, DV, T, Pr, RS, HR
Altitude (masl)	2577	2580	2552	2589
Height of sampling (m)	4.6	7.0	4.6	3.0
Type of monitoring station	Background	Background	Traffic	Background

Table 1. *Cont.*

Characteristic	Monitoring Stations			
	CAR	**KEN**	**LAF**	**TUN**
Mean annual relative humidity (%)	67.6	63.1	63.2	62.6
Mean annual precipitation (mm)	1148	797	1147	980
Mean annual temperature (°C)	14.9	15.8	14.4	14.9
Mean annual wind speed (m/s)	1.21	2.15	1.87	1.36
Predominant annual wind direction (°)	204 (SSW)	196 (S)	140 (SE)	175 (S)
Land use (%)	R: 54.9	R: 38.4	R: 53.1	R: 41.9
	I: 4.40	I: 5.80	I: 7.10	I: 0.60
	D: 3.80	D: 37.1	D: 10.0	D: 8.90
	C: 9.60	C: 18.4	C: 5.20	C: 31.3
	P: 8.30	P: 0.20	P: 2.80	P: 17.0
Land category (%)	Urban: 100	Urban: 93.5	Urban: 95.8	Urban: 71.5
		Urban sprawl: 6.55	Urban sprawl: 4.14	Protection: 28.5
Population density (Inhabitants/Ha)	123	268	227	183

Note: VV—wind speed, DV—wind direction, T—temperature, Pr—precipitation, RS—solar radiation, Ps—atmospheric pressure, R—residential, I—industrial, D—residential and services, C—commercial, and P—protection.

2.2. Data Collection

The time series data procured from the monitoring stations provided hourly information on the PM_{10} and $PM_{2.5}$ concentrations, relative humidity (%), precipitation (mm), temperature (°C), wind speed (m/s), and wind direction (°). This study spanned a period of five years, from 1 January 2017 to 31 December 2021, a timeline chosen in accordance with the occurrence of the COVID-19 isolation episodes within the megacity. The method employed for the collection of PM_{10} and $PM_{2.5}$ samples, aimed at determining the presence of inorganic compounds in the air, adhered to the guidelines established by U.S. EPA/625/R-96/010a [44]. Furthermore, the monitoring system was designed in compliance with the guidelines set forth in CFR 40, Part 50, Appendices J and L, for the automatic measurement of PM_{10} (Met One Bam 1020) and $PM_{2.5}$ (Thermo Scientific FH62C14-DHS, MA, USA) [45]. The system utilized Beta Ray Attenuation as the principle of measurement.

2.3. Data Analysis

The analysis of the data was conducted in three phases. In the first phase, an exploratory analysis of the hourly time series of atmospheric pollutants and meteorological parameters was carried out. Initially, the non-normal distribution (p-value > 0.050) of the time series was examined using a Kolmogorov–Smirnov test [46]. The correlation between the variables considered was also studied using Spearman's coefficient [47]. These correlations between PM_{10} and $PM_{2.5}$ and the meteorological parameters allowed for the study of the influence of meteorological conditions and anthropogenic activity due to COVID-19 isolation. Three scenarios of human activity were considered: (1) pre-isolation, (2) isolation, and (3) historical. Descriptive statistics (mean, median, and standard deviation) were calculated for the time series under study. The IBM SPSS Statistics V.25.0 software [48] was used in this study. Lastly, wind roses, pollution roses, and polar roses were developed for the PM_{10} and $PM_{2.5}$ concentrations at each of the monitoring stations using the OpenAir package of the R software [12,15].

In the second phase, the missing data in the time series of atmospheric pollutants and meteorological parameters were filled in. It was previously confirmed that all the time series had more than 75% of the data. The random nature of the missing data was detected using the Visualization and Imputation of Missing Values (VIM) package of the R 4.2.1 software [49]. The missing data were filled in using the Multivariate Imputation by

Chained Equations (MICE) and Nonparametric Missing Value Imputation using Random Forest (MissForest) packages of the R 4.2.1 software [50]. The MICE package used various methods (Predictive Mean, Bayesian Linear Regression, and Logistic Regression) to fill in the missing data [51]. The MissForest package filled in the missing data by creating random forests with the observed data, then iterated again until the minimum error was obtained [52].

In the third phase, the ARIMA models were developed for the PM_{10} and $PM_{2.5}$ concentrations. The timescales considered were as follows: daily (24 h moving average), weekly (120 h moving average), and monthly (720 h moving average). The development of the ARIMA models also considered three scenarios: (1) before the first isolation (E1), (2) during the different types of isolation (E2.1 = strict, E2.2 = sectorized, and E2.3 = flexible), and (3) the historical trend (E3) (Table 2). The development of the ARIMA models was based on the methodology reported by Box and Jenkins [53]. This methodology considered the following stages: identification, parameter estimation, assumption verification, and model use [53]. From the temporal length of the isolation scenarios considered (less than 5 months), it was assumed in this study that the weekly timescale was the most appropriate. The ARIMA modeling of the PM_{10} and $PM_{2.5}$ concentrations was performed using IBM SPSS Statistics V.25.0 software [54].

During the development of the ARIMA models, the PM concentration time series underwent differencing and transformation (square root and logarithmic) according to their time structure. This process was performed to obtain a stationary series (independence). Subsequently, the model identification and parameter estimation were carried out, leading to the determination of the p, d, and q orders of the ARIMA models. The previous stages were carried out using the IBM SPSS Statistics V.25.0 Expert Modeler Tool [54]. Once the p, d, and q terms were identified, compliance with the Ljung–Box statistic (p-value > 0.05) was verified in the model obtained. Compliance with the Ljung–Box test indicated that the residuals of the model were equal or close to zero and that its variance was constant, becoming white noise, confirming the development of a model that adequately described the observed variable [33,55]. If the Ljung–Box statistic was not met, the p, d, and q terms of the initial model were modified until a suitable ARIMA model was obtained. Once the ARIMA model was identified, estimated, and verified, the goodness of fit coefficients (RMSE: root mean square error, MAE: mean percentage error, MAPE: maximum mean percentage error, and R^2) were reviewed, with emphasis placed on the Bayesian Information Criterion (BIC) [54]. This last statistic allowed the selection of the model with the highest goodness of fit using the fewest possible terms [56]. All statistics were estimated with a confidence level of 95%.

Table 2. ARIMA analysis scenarios for COVID-19 isolation.

Scenario		Start Date	End Date	Characteristics
Pre-isolation E1		1 January 2020	25 March 2020	Without any type of isolation. Usual behavior of anthropic activities.
Isolation E2	Strict E2.1	25 March 2020	27 August 2020	Controlled outflow for primary activities (health, services, and supply). 41% reduction in population mobility [57]. 85–90% reduction in vehicular transport. Staggered reduction in isolation (12 June 2023). 65–70% reduction in vehicular transport [58].
	Sectorized E2.2	5 January 2021	2 February 2020	Weekly isolation by sector in the city. 63.3% of work activity was remote. Access to closed spaces, stores, and public areas continued to be restricted [59].
	Flexible E2.3	10 April 2020	7 June 2020	Reactivation of the economic sectors of manufacturing, construction, restaurants, and educational centers. Control of maximum capacity in transportation, public places, and commercial establishments. By the end of the scenario, general isolation was repealed [60].

Table 2. *Cont.*

Scenario		Start Date	End Date	Characteristics
Historical E3	Strict E3.1	25 March 2017–2019	27 August 2017–2019	Historical concentrations of atmospheric pollutants for the same periods (without COVID-19). Three previous years according to other authors' considerations [14,61,62].
	Sectorized E3.2	5 January 2017–2019	2 February 2017–2019	
	Flexible E3.3	10 April 2017–2019	7 June 2017–2019	

Following the development of the ARIMA models, the time series simulated under scenarios E1, E2, and E3 were examined. With this information on the PM_{10} and $PM_{2.5}$ concentrations, the following analyses were performed: (1) A non-parametric comparison (a Mann–Whitney U test) [63] was conducted on the simulated time series for scenarios E2 and E3 (E2.1–E3.1, E2.2–E3.2, and E2.3–E3.3). This allowed for an evaluation of similar behavior between the time series of the isolation period (with COVID-19) and the historical period (without COVID-19). (2) The percentage changes were calculated for the simulated weekly concentrations in the short and long term. The short-term percent changes were obtained by comparing the weekly PM_{10} and $PM_{2.5}$ concentrations between scenarios E1 (pre-isolation) and E2 (isolation): E1–E2.1, E1–E2.2, and E1–E2.3. The long-term percent change was obtained by comparing the weekly PM_{10} and $PM_{2.5}$ concentrations between scenarios E2 (isolation) and E3 (historical): E2.1–E3.1, E2.2–E3.2, and E2.3–E3.3. The aim was to quantify the change in the trends of the PM_{10} and $PM_{2.5}$ concentrations during the isolation scenarios [64]. (3) The behavior of the *p*, *d*, and *q* terms and the goodness of fit statistics (BIC, RMSE, MAPE, and R^2) of the ARIMA models developed for both the short and long term were analyzed. With this, the occurrence of changes in the ARIMA temporal structure of the weekly PM_{10} and $PM_{2.5}$ concentrations during the COVID-19 isolation was evaluated. This was done in relation to the other established analysis scenarios.

3. Results and Discussion

3.1. PM Concentrations

The results showed that the lowest PM concentrations at the monitoring stations were observed during scenario E2.1 (strict isolation): CAR/PM_{10} = 15.7 $\mu g/m^3$, KEN/PM_{10} = 33.9 $\mu g/m^3$, LAF/PM_{10} = 17.0 $\mu g/m^3$, TUN/PM_{10} = 25.9 $\mu g/m^3$, $CAR/PM_{2.5}$ = 9.38 $\mu g/m^3$, $KEN/PM_{2.5}$ = 16.9 $\mu g/m^3$, $LAF/PM_{2.5}$ = 9.40 $\mu g/m^3$, and $TUN/PM_{2.5}$ =10.3 $\mu g/m^3$ (Figure 2). This trend was possibly associated with the strict isolation measures and temporary closure of non-primary economic activities observed during this scenario. However, sudden increases in the PM concentrations were observed between the months of March–April and June–July 2020, which were probably associated with regional PM transport events (e.g., forest biomass burning) [25]. The above trend was more evident in PM_{10} compared to $PM_{2.5}$. During the E2.3 flexible isolation scenario, a decrease in the PM concentrations was also observed, although this decrease was smaller compared to the E2.1 scenario (PM_{10} = 6.92%; $PM_{2.5}$ = 5.79%). This lower reduction in the PM concentrations was possibly associated with the controlled reactivation of the economic sectors of manufacturing, construction, restaurants, and educational centers, due to flexible isolation (Table 2) [59].

The findings showed that the highest concentrations of PM at the monitoring stations were observed during the E1 scenario (pre-isolation): CAR/PM_{10} = 31.3 $\mu g/m^3$, KEN/PM_{10} = 47.8 $\mu g/m^3$, LAF/PM_{10} = 36.8 $\mu g/m^3$, TUN/PM_{10} = 49.9 $\mu g/m^3$, $CAR/PM_{2.5}$ = 20.6 $\mu g/m^3$, $KEN/PM_{2.5}$ = 29.6 $\mu g/m^3$, $LAF/PM_{2.5}$ = 22.9 $\mu g/m^3$, and $TUN/PM_{2.5}$ = 22.1 $\mu g/m^3$ (Figure 2). During the E2.2 scenario of sectorized isolation, the PM concentrations also tended to increase, although this increase was smaller compared to the E1 scenario (PM_{10} = 23.9%; $PM_{2.5}$ = 45.3%). The E2.2 scenario showed a different behavior in relation to the other isolation scenarios (E2), as increases in the PM concentrations were observed (Table 2). This trend was similar to that observed during the E3.2

scenario of historical behavior, although the increases in the PM concentrations were lower (PM_{10} = 21.3%; $PM_{2.5}$ = 23.0%). The results suggested that this trend was related to the period of occurrence of these two scenarios (E2.2 and E3.2). That is, the two scenarios developed during the first three months of each year, a period of time in which it was common to detect episodes of regional PM transport (e.g., forest fires and Saharan dust) and meteorological conditions where there was a decrease in precipitation and wind speed [23,25]. These meteorological conditions probably did not favor the dispersion of pollutants, which facilitated the formation and accumulation of PM in the urban atmosphere. This behavior has also been reported in cities under similar meteorological conditions [65].

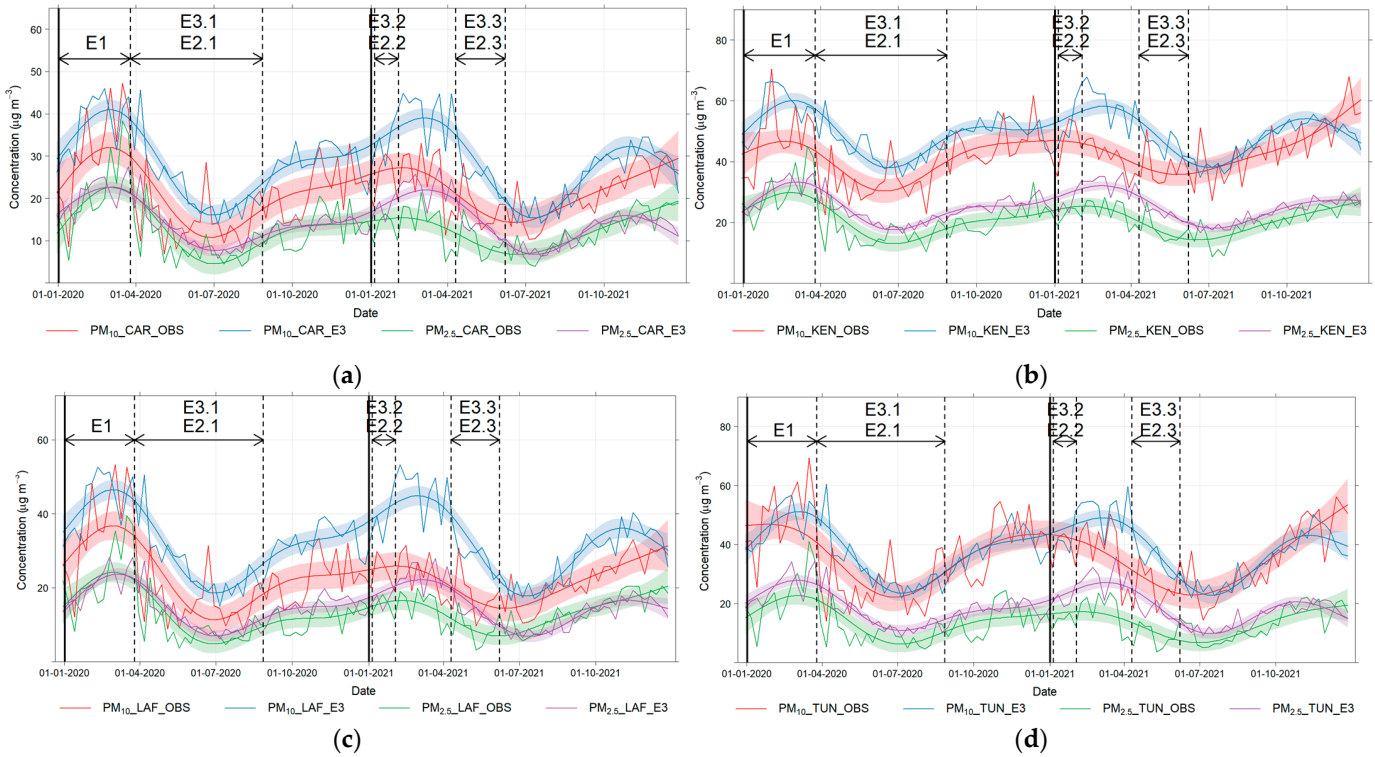

Figure 2. Behavior of PM_{10} and $PM_{2.5}$ concentrations during the study scenarios (E1, E2, and E3): (**a**): CAR, (**b**) KEN, (**c**) LAF, and (**d**) TUN. OBS: observed concentrations during the study scenarios (E1 and E2) and E3: observed historical concentrations.

The findings showed strong positive correlations between the PM_{10} and $PM_{2.5}$ concentrations (Spearman rs between 0.71 and 0.89) at all the monitoring stations during the E3 scenario (historical scenario). This trend suggested a similar historical behavior in the formation and transport of PM_{10} (the coarse fraction) and $PM_{2.5}$ (the fine fraction), which has also been reported in other studies [66]. However, during the isolation scenarios (E2), a decrease in the Spearman correlation coefficients (rs between 0.50 and 0.76) was evidenced. The previous trend suggested a change in the activity of PM_{10} and $PM_{2.5}$ pollution sources during the isolation scenarios. On average, there was a 20% decrease in the magnitude of the Spearman correlation coefficients during the isolation scenarios (E2). This decrease in the correlation between the PM_{10} and $PM_{2.5}$ concentrations was possibly associated with the intervention of external factors during the formation and transport of PM. There were studies that associated this trend with the following external factors: (1) differential meteorological conditions that increased the concentrations of a specific PM fraction [48,67]; (2) regional PM transport events, which increased PM concentrations [68,69]; and (3) changes in the baseline level of atmospheric emissions [11,70]. Therefore, the results suggested that the possible changes in the PM concentrations during the isolation scenarios (E2) could not be attributed exclusively to the implemented restrictions (Table 2).

3.2. Meteorological Analysis

The results showed that the lowest relative humidity occurred during the E2.2 scenario of sectorized isolation (CAR = 64.7%, KEN = 59.9%, LAF = 60.2%, and TUN = 57.8%). This scenario also showed the least precipitation (CAR = 15.1 mm, KEN = 20.5 mm, LAF = 10.3 mm, and TUN = 9.20 mm). The E2.2 scenario of sectorized isolation showed a different behavior in the PM concentrations compared to the other isolation scenarios (E2). That is, an increase in the PM concentrations was observed, possibly associated with the decrease in precipitation and relative humidity, which probably led to less favorable conditions for the vertical dispersion of this air pollutant, similar conditions to those reported in Milan (Italy) [60] and Sao Paulo (Brazil) [64] during the COVID-19 isolation. This trend was also similar to that observed during the E3.2 scenario of historical behavior, although the increases in the PM concentrations were lower in the E2.2 scenario (PM_{10} = 21.3%; $PM_{2.5}$ = 23.0%). On the other hand, the findings showed that the highest relative humidity occurred during the E2.1 (CAR = 67.2%, KEN = 63.0%, LAF = 62.6%, and TUN = 62.7%) and E2.3 (CAR = 67.6%, KEN = 63.9%, LAF = 64.3%, and TUN = 63.9%) scenarios of strict and flexible isolation, respectively. These two scenarios were also the ones that showed the highest precipitation (351/233 mm, 983/370 mm, 202/293 mm, and 376/264 mm, respectively). The results suggested that during the E2.1 scenarios of strict isolation and E2.3 of flexible isolation, the decrease in the PM concentrations were, in part, influenced by the observed meteorological conditions, which favored the washing of the pollutants in the atmosphere [17]. However, the effect on the PM concentrations of the restrictions established during these two isolation scenarios (Table 2) should not be forgotten.

On average, the findings showed that wind speeds tended to be slightly higher (4.74%) during the isolation scenarios (E2) compared to the historical scenarios (E3). However, a Mann–Whitney U test allowed the visualization of the non-existence of significant differences (p-value > 0.050) in the wind speed between these two scenarios. In relation to the wind direction, the results showed a predominance from the SE at all study stations. Nevertheless, as there were isolation scenarios less than five months, the predominant wind direction tended to change during these periods (SSE, SSW, S, and NE). The findings showed that during the scenario of the lower concentrations of PM_{10} and $PM_{2.5}$ (E2.1—strict isolation) the predominant wind direction at the monitoring stations was between SSE and SE. During the E2.3 scenario (flexible isolation), a decrease in the PM concentrations was also observed, as was a predominance in the wind direction between SSE and E. In general, the results suggested that during the scenarios of lower PM concentrations (E2.1 and E2.3) the wind tended to come from the east. In contrast, during the scenario of higher PM concentrations (E1—pre-isolation) the predominant wind direction at the monitoring stations tended to be between WNW and SW. During the E2.2 scenario, the PM concentrations tended to increase. Under this scenario, the predominant wind direction tended to be between SSW and WNW. This trend was similar to that observed during the E3.2 scenario of historical behavior, in which an increase in the PM concentrations was evidenced. In general, the findings suggested that during the scenarios of increasing PM concentrations (E1, E2.2, and E3.2) the wind tended to come from the west. This trend was more evident for $PM_{2.5}$ than for PM_{10} (Figure 3). Lastly, the results suggested that the E2.2 scenario of sectorized isolation (where there was an increase in the PM concentration) could have been influenced by the regional transport of PM (with the forest biomass burning). Other authors have also reported scenarios where urban PM concentrations were influenced by adverse weather conditions that caused the dispersion of air pollutants [67,70].

The results showed that the meteorological variable that best correlated with the PM_{10} ($rs \leq 0.32$) and $PM_{2.5}$ ($rs \leq 0.32$) concentrations during the historical scenario (E3) was wind direction. Significant positive correlations from weak to medium (rs for PM_{10} up to 0.32 and rs for $PM_{2.5}$ up to 0.32) were observed with this variable. However, during the isolation scenarios (E2), these correlations tended to increase. This increase in correlations was greater for $PM_{2.5}$ compared to PM_{10}. Significant positive correlations for PM_{10} and $PM_{2.5}$

up to 0.40 and 0.52 (around medium), respectively, were evidenced. The results suggested that during the isolation scenario (E2) there was possibly an external contribution of PM (due to regional transport) in the megacity under study, especially for the concentrations in the southwest (KEN) and south (TUN) of the megacity. From the observed increase in the correlations, the external contribution of $PM_{2.5}$ was possibly greater compared to the contribution of PM_{10}. Borhani et al. [66] reported a similar scenario in Tehran (Iran), where during the isolation, regional transport contributed increases in suspended particles, especially for $PM_{2.5}$, which came from industrial and stationary emission sources. The findings also suggested that the increase in the PM concentrations during the E2.2 scenario (sectorized isolation) compared to the other isolation scenarios (E2.1 and E2.3) could be related to the episodes of regional PM transport and increases in the PM emission levels in the sectors of the megacity that had no restrictions (Table 2). Lastly, this study showed very weak or non-significant correlations of the PM concentrations with precipitation, relative humidity, wind speed, and temperature during the isolation scenarios considered.

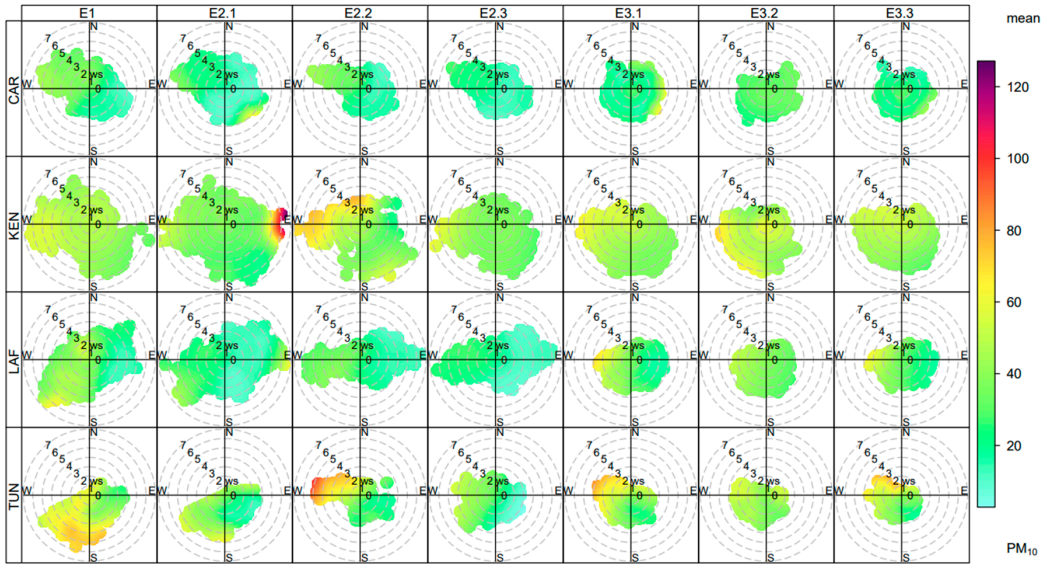

(**a**)

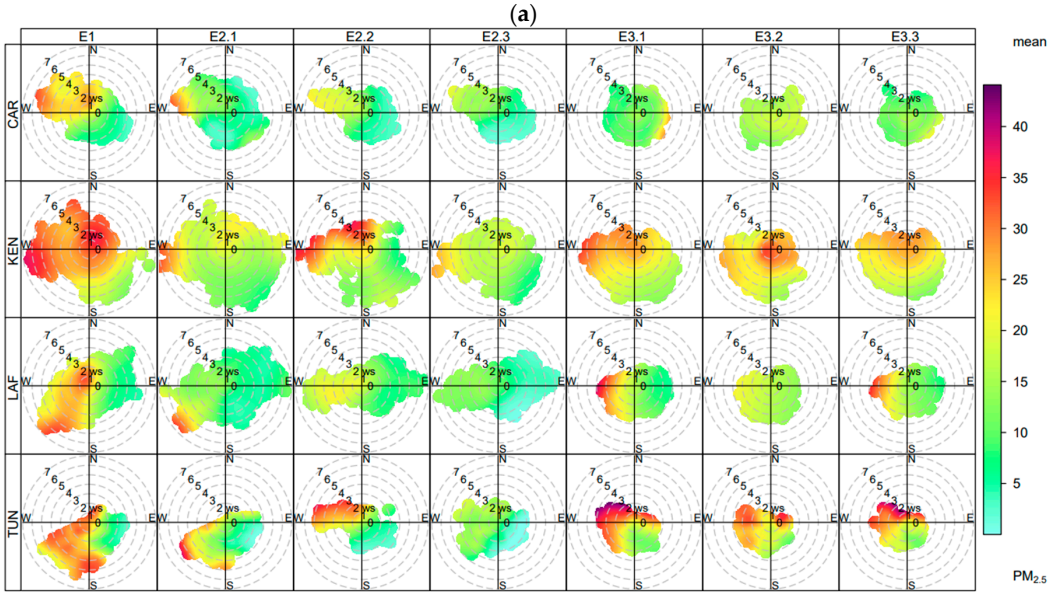

(**b**)

Figure 3. Polar plots for (**a**) PM_{10} and (**b**) $PM_{2.5}$ concentrations for each monitoring station and analysis scenario. WS: wind speed (m/s).

3.3. Short- and Long-Term Analysis

ARIMA models were developed for each of the considered scenarios (E1, E2, and E3). The models were developed under a weekly timeframe (168 h moving average; Table 3). The results, based on a Kolmogorov–Smirnov test, showed that all the variables exhibited a non-normal distribution (p-value < 0.05).

Table 3. ARIMA models developed for PM_{10} and $PM_{2.5}$ concentrations during the scenarios considered.

Station		AR (p)	I (d)	MA (q)	Transformation	R^2	MAE	RMSE	MAPE	Q′	p-Value	DF	BIC
						E1							
CAR	PM_{10}	6	1	2	Square root	0.999	0.043	0.057	0.151	18.099	0.053	10	−5.689
	$PM_{2.5}$	11	2	1	None	0.999	0.039	0.055	0.219	11.461	0.075	6	−5.762
KEN	PM_{10}	2	2	1	None	0.999	0.056	0.079	0.121	20.683	0.147	15	−5.060
	$PM_{2.5}$	2	1	1	None	0.999	0.059	0.078	0.213	11.037	0.750	15	−5.086
LAF	PM_{10}	3	2	7	None	0.999	0.069	0.099	0.193	14.380	0.072	8	−4.584
	$PM_{2.5}$	0	2	7	Square root	0.999	0.055	0.073	0.271	17.432	0.096	11	−5.207
TUN	PM_{10}	2	1	1	None	0.999	0.095	0.132	0.199	16.991	0.319	15	−4.027
	$PM_{2.5}$	2	1	1	None	0.999	0.046	0.067	0.244	19.117	0.208	15	−5.381
						E2.1							
CAR	PM_{10}	1	1	3	Natural logarithm	0.999	0.028	0.040	0.199	21.192	0.097	14	−6.440
	$PM_{2.5}$	1	1	8	Natural logarithm	0.999	0.026	0.038	0.347	14.635	0.101	9	−6.525
KEN	PM_{10}	1	2	3	Natural logarithm	0.999	0.042	0.056	0.130	16.815	0.266	14	−5.764
	$PM_{2.5}$	0	2	6	None	0.999	0.046	0.059	0.296	7.864	0.796	12	−5.628
LAF	PM_{10}	1	2	4	Natural logarithm	0.999	0.030	0.044	0.197	10.617	0.643	13	−6.243
	$PM_{2.5}$	0	2	6	None	0.999	0.024	0.034	0.316	12.118	0.436	12	−6.746
TUN	PM_{10}	1	1	5	Square root	0.999	0.064	0.092	0.267	17.624	0.128	12	−4.755
	$PM_{2.5}$	0	2	12	None	0.999	0.033	0.046	0.385	4.195	0.650	6	−6.107
						E3.1							
CAR	PM_{10}	2	1	1	None	0.999	0.040	0.053	0.183	17.074	0.314	15	−5.869
	$PM_{2.5}$	1	2	13	Square root	0.999	0.024	0.032	0.225	1.909	0.752	4	−6.854
KEN	PM_{10}	7	1	1	Natural logarithm	0.999	0.046	0.062	0.106	14.788	0.140	10	−5.533
	$PM_{2.5}$	1	1	13	Natural logarithm	0.999	0.032	0.042	0.146	6.420	0.170	4	−6.318
LAF	PM_{10}	1	1	12	None	0.999	0.043	0.058	0.172	9.572	0.088	5	−5.664
	$PM_{2.5}$	0	2	15	None	0.999	0.027	0.036	0.257	1.841	0.606	3	−6.598
TUN	PM_{10}	4	1	1	Natural logarithm	0.999	0.052	0.070	0.168	16.950	0.202	13	−5.293
	$PM_{2.5}$	1	1	5	Natural logarithm	0.999	0.035	0.047	0.233	12.616	0.398	12	−6.115
						E2.2							
CAR	PM_{10}	0	2	9	Natural logarithm	0.999	0.061	0.083	0.237	10.085	0.344	9	−4.844
	$PM_{2.5}$	1	2	1	None	0.999	0.033	0.046	0.254	24.188	0.085	16	−6.108
KEN	PM_{10}	0	2	1	None	0.999	0.054	0.075	0.118	25.517	0.084	17	−5.172
	$PM_{2.5}$	0	2	3	None	0.999	0.056	0.073	0.258	12.180	0.665	15	−5.192
LAF	PM_{10}	1	2	4	Natural logarithm	0.999	0.054	0.075	0.216	17.942	0.160	13	−5.112
	$PM_{2.5}$	0	2	7	Natural logarithm	0.999	0.047	0.061	0.297	18.559	0.069	11	−5.485
TUN	PM_{10}	4	2	1	Natural logarithm	0.999	0.087	0.125	0.229	6.561	0.087	3	−3.959
	$PM_{2.5}$	1	1	1	None	0.999	0.043	0.060	0.316	10.774	0.823	16	−5.596
						E3.2							
CAR	PM_{10}	1	2	1	Square root	0.999	0.040	0.054	0.129	7.891	0.952	16	−5.790
	$PM_{2.5}$	0	2	2	None	0.999	0.026	0.035	0.157	25.930	0.055	16	−6.676
KEN	PM_{10}	1	1	0	Natural logarithm	0.999	0.053	0.071	0.108	14.318	0.644	17	−5.261
	$PM_{2.5}$	2	1	1	Natural logarithm	0.999	0.035	0.046	0.141	10.817	0.765	15	−6.094
LAF	PM_{10}	0	2	6	Natural logarithm	0.999	0.052	0.069	0.144	20.223	0.063	12	−5.247
	$PM_{2.5}$	1	1	8	Natural logarithm	0.999	0.030	0.038	0.186	14.734	0.098	9	−6.403

Table 3. *Cont.*

Station		AR (*p*)	I (*d*)	MA (*q*)	Transformation	R^2	MAE	RMSE	MAPE	Q′	*p*-Value	DF	BIC
						E3.2							
TUN	PM_{10}	1	1	0	None	0.998	0.058	0.077	0.148	24.639	0.103	17	−5.116
	$PM_{2.5}$	1	1	7	Natural logarithm	0.999	0.038	0.052	0.184	8.940	0.538	10	−5.809
						E2.3							
CAR	PM_{10}	1	2	4	None	0.999	0.050	0.074	0.300	20.424	0.085	13	−5.179
	$PM_{2.5}$	1	1	2	Square root	0.999	0.028	0.039	0.303	18.976	0.215	15	−6.487
KEN	PM_{10}	0	2	14	Square root	0.999	0.053	0.073	0.142	8.073	0.089	4	−5.136
	$PM_{2.5}$	1	2	1	None	0.999	0.052	0.068	0.316	12.971	0.675	16	−5.369
LAF	PM_{10}	8	2	8	Natural logarithm	0.999	0.037	0.054	0.216	5.448	0.066	2	−5.741
	$PM_{2.5}$	2	2	2	None	0.999	0.028	0.039	0.394	13.060	0.522	14	−6.440
TUN	PM_{10}	1	1	12	Natural logarithm	0.999	0.075	0.107	0.303	5.307	0.380	5	−4.394
	$PM_{2.5}$	1	1	15	Square root	0.999	0.034	0.049	0.450	2.709	0.258	2	−5.921
						E3.3							
CAR	PM_{10}	1	1	4	None	0.999	0.044	0.057	0.172	15.500	0.277	13	−5.694
	$PM_{2.5}$	2	1	1	None	0.999	0.028	0.035	0.207	18.587	0.233	15	−6.656
KEN	PM_{10}	1	1	1	None	0.999	0.051	0.067	0.110	19.092	0.264	16	−5.375
	$PM_{2.5}$	1	1	7	Natural logarithm	0.999	0.035	0.046	0.150	8.840	0.547	10	−6.114
LAF	PM_{10}	1	1	12	None	0.999	0.046	0.061	0.159	5.433	0.365	5	−5.514
	$PM_{2.5}$	2	1	7	None	0.999	0.030	0.039	0.227	16.431	0.058	9	−6.441
TUN	PM_{10}	1	1	11	Natural logarithm	0.999	0.057	0.074	0.164	7.041	0.317	6	−5.128
	$PM_{2.5}$	1	1	8	Natural logarithm	0.999	0.038	0.050	0.219	8.781	0.458	9	−5.921

Note: AR—autoregressive, I—integrated, MA—moving average, RMSE—root mean square error, MAE—mean percentage error, MAPE—maximum mean percentage error, R2—determination coefficient, Q′—Ljung–Box statistic, *p*-value—*p*-value, DF—degrees of freedom, and BIC—Bayesian Information Criterion.

The results showed that, during scenario 2.1 of strict isolation, the greatest short-term reduction (compared to E1) was observed in the simulated concentrations of PM_{10} and $PM_{2.5}$. On average, the short-term reductions in the PM_{10} and $PM_{2.5}$ concentrations for the LAF, CAR, TUN, and KEN stations were as follows: 55.7/60.6%, 51.9/56.5%, 49.9/54.8%, and 31.6/44.1%, respectively (Figure 4). In relation to the long-term trend (compared to E3.1), the findings showed a smaller reduction in the simulated concentrations of PM_{10} and $PM_{2.5}$ during scenario E2.1. On average, the long-term reductions in the PM_{10} and $PM_{2.5}$ concentrations for the CAR, LAF, KEN, and TUN stations were as follows: 34.2/24.7%, 37.3/25.3%, 24.4/25.2%, and 21.7/37.9%, respectively. The findings confirmed that there was a short- and long-term reduction in the PM concentrations during scenario E2.1 of strict isolation. Indeed, this trend was primarily related to the strict isolation measures implemented due to COVID-19. A Mann–Whitney U test indicated the existence of significant differences (p-value > 0.050) between the simulated PM concentrations for scenarios E2.1 and E3.1. This behavior possibly confirmed the incidence of the implemented strict isolation measures. However, the influence of factors such as the regional transport of PM from hotspots and the emissions from industrial activities external to the megacity was not ruled out [14,71].

The findings showed that the greatest short-term reductions in the simulated PM concentrations during the E2.1 scenario of strict isolation tended to occur for $PM_{2.5}$ compared to PM_{10}. On average, the short-term reductions (compared to E1) in the $PM_{2.5}$ and PM_{10} concentrations during the E2.1 scenario were as follows (significant differences, p-value < 0.050): 54/47.3%, respectively (Figure 4). Indeed, this short-term trend in the $PM_{2.5}$ concentrations was possibly related to the established strict isolation restrictions. In other words, the strict isolation measures had a greater short-term effect on $PM_{2.5}$ compared to PM_{10}. In the long term (compared to E3.1), the reduction in the $PM_{2.5}$ and PM_{10} concentrations was similar (no significant differences, p-value = 0.235): 28.3/29.4%, respectively. The results suggested that this long-term trend was possibly more associated with those

regional PM transport processes that typically occurred during the months of March–April and June–July [21]. These regional transport processes possibly tended to increase the $PM_{2.5}$ concentrations, which made the decrease in the $PM_{2.5}$ and PM_{10} concentrations similar. Short-term measures were important for assessing immediate exposure and health risks, while long-term measures were essential for understanding trends and the cumulative effects of air pollution over time [64].

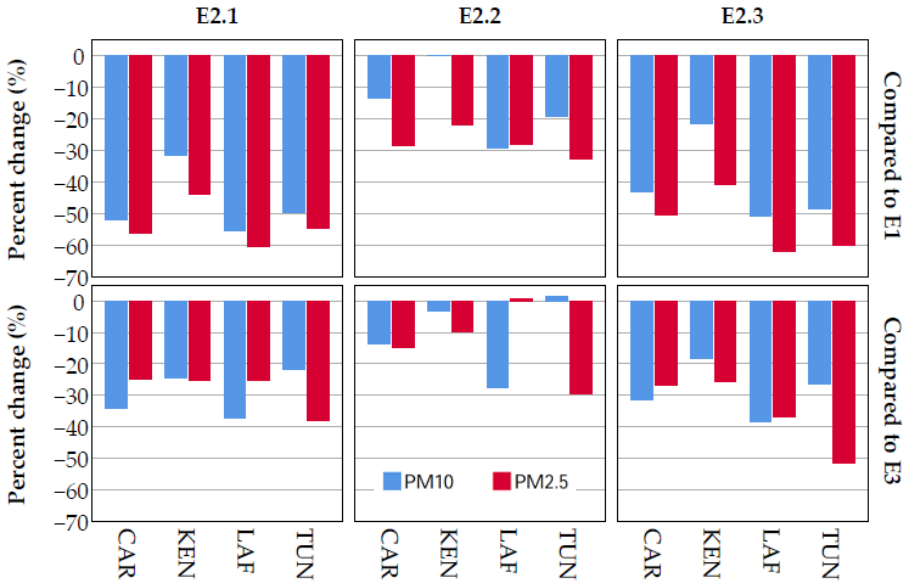

Figure 4. Average percent change in simulated PM_{10} and $PM_{2.5}$ concentrations during the E2 isolation scenario. E2.1—strict isolation, E2.2 —sectorized isolation, and E2.3—flexible isolation. E1—short term and E3—long term.

In the E2.2 scenario of sectorized isolation, the results revealed a short-term reduction (compared to E1) in the simulated PM concentrations (significant differences, p-value < 0.050). The reduction in the PM_{10} and $PM_{2.5}$ concentrations for the LAF, TUN, and CAR stations were as follows: 29.4/28.0%, 19.3/32.6%, and 13.3/28.5%, respectively. On the other hand, the KEN station did not show a short-term reduction (no significant difference, p-value = 0.670) in the PM_{10} concentrations (0.01%), although it did experience a reduction in the $PM_{2.5}$ concentrations (21.8%). In general, in the long term (compared to E3.2), the PM_{10} concentrations also tended to decrease during the E2.2 scenario of sectorized isolation (significant differences, p-value < 0.050). The decrease in the concentrations for the LAF, CAR, and KEN stations were as follows: 27.6%, 13.8%, and 3.11%, respectively. At the TUN station, no reduction was observed (no significant difference, p-value = 0.753) in the PM_{10} concentration; that is, a slight increase of 1.50% in the PM_{10} concentration was evidenced. In relation to the $PM_{2.5}$ concentrations, the results showed reductions of 29.4%, 14.9%, and 9.79% in the concentrations for the TUN, CAR, and KEN stations, respectively. At the LAF station, no reduction was observed (no significant difference, p-value = 0.510) in the $PM_{2.5}$ concentration; that is, a slight increase of 0.55% was evidenced.

Therefore, the results revealed that the greatest short-term reductions (compared to E1) in the simulated PM concentrations during the E2.2 scenario of sectorized isolation tended to occur for $PM_{2.5}$ rather than PM_{10}. On average, the short-term reductions in the $PM_{2.5}$ and PM_{10} concentrations during the E2.2 scenario were as follows: 29.7/20.7%, respectively (Figure 4). However, at the KEN station, no significant short-term reduction was observed in the PM_{10} concentrations, but for the $PM_{2.5}$ concentrations this reduction was significant during the E2.2 scenario of sectorized isolation. In the long term (compared to E3.2), the reduction in the $PM_{2.5}$ and PM_{10} concentrations were as follows: 18.0/14.8%, respectively. However, at the TUN and LAF stations, no reductions were observed in the PM_{10} and $PM_{2.5}$ concentrations. These short- and long-term trends in the reduction in the concentrations

during the E2.2 scenario were possibly related to the established sectorized isolation measures (Table 2). In other words, under this scenario of sectorized isolation, the short- and long-term reductions in the $PM_{2.5}$ (45/36.4%) and PM_{10} (56.2/49.7%) concentrations were smaller compared to the E2.1 scenario of strict isolation.

Additionally, it was observed during the E2.2 scenario of sectorized isolation that in the central (CAR), western (LAF), and southern (TUN) zones of the megacity, reductions in the PM concentrations occurred both in the short and long term. In the southwestern zone (KEN), the smallest reductions in the PM concentrations were observed. Thus, the results suggested that in the center, west, and south of the megacity, the restrictions due to sectorized isolation had a greater effect compared to the southwestern zone. This spatial trend was possibly related to the influence of the sectorized isolation measures and land use [40,72]. Moreover, during this scenario, climatic conditions possibly also influenced the smaller reduction in the PM concentrations. That is, a higher occurrence of low wind speeds (<1m/s), a decrease in precipitation, the development of thermal inversions, and the regional transport of PM were reported [7,73,74].

In the E2.3 flexible isolation scenario, the results evidenced a short-term reduction (compared to E1) in the simulated PM concentrations (significant differences, p-value < 0.050). The average reduction in the PM_{10} and $PM_{2.5}$ concentrations for the LAF, TUN, CAR, and KEN stations were as follows: 50.9/62.2%, 48.6/60.3%, 42.9/50.6%, and 21.5/40.8%, respectively. In the long term (compared to E3.3), the findings also showed a reduction in the simulated PM_{10} and $PM_{2.5}$ concentrations during the E2.3 scenario. On average, the reductions in the PM_{10} and $PM_{2.5}$ concentrations for the TUN, LAF, CAR, and KEN stations were as follows: 26.4/51.4%, 38.3/36.8%, 31.6/26.6%, and 18.4/25.7%, respectively. The findings suggested that there was a short- and long-term reduction in the PM concentrations during the E2.3 flexible isolation scenario. A Mann–Whitney U test suggested the existence of significant differences (p-value > 0.050) between the simulated PM concentrations for the E2.3 and E3.3 scenarios. Indeed, this trend was mainly related to the flexible isolation measures implemented as a result of COVID-19. For example, it was reported that 63.3% of the population worked remotely [60]. However, meteorology possibly also influenced the reduction in the PM concentrations during this flexible isolation scenario.

The results revealed that the greatest short-term reductions (compared to E1) in the simulated PM concentrations during the E2.3 flexible isolation scenario tended to occur for $PM_{2.5}$ compared to PM_{10}. On average, the short-term reductions in the $PM_{2.5}$ and PM_{10} concentrations during the E2.3 flexible isolation scenario were as follows: 53.5/41%, respectively (Figure 3). In the long term (compared to E3.3), the reduction in the $PM_{2.5}$ and PM_{10} concentrations were as follows: 35.1/28.7%, respectively. Indeed, these short- and long-term trends in the reduction in the concentrations during the E2.3 scenario were possibly related to the established flexible isolation measures (Table 2), the observed climatic conditions, and the regional contribution of PM. Under this flexible isolation scenario, the short- and long-term reductions in the $PM_{2.5}$ (1.01 times lower and 1.24 times higher) and PM_{10} (1.15 times lower and 1.02 times lower) concentrations were similar or greater comparatively with the E2.1 strict isolation scenario.

3.4. ARIMA Models

The analysis scenarios considered were comparatively evaluated based on variations in the autoregressive (AR), difference (I), and moving averages (MA) terms of the developed ARIMA models.

In relation to the E2.1 strict isolation scenario, the results showed AR = 1 in the ARIMA models developed for the PM_{10} concentrations. In the short term (E1), the findings showed AR terms between 2 and 6 for the PM_{10} concentrations (Table 3). The results suggested that, in the short term, strict isolation measures tended to decrease the magnitude of the AR term (phenomenon memory). In other words, strict isolation measures tended to reduce the persistence over time of the PM_{10} concentrations. Persistence in an ARIMA model refers

to the model's ability to capture and predict the temporal relationship between the past and present values of a time series [31]. High persistence could indicate a time series with a trend or pattern that persisted over time, while low persistence could indicate a more volatile time series or with more abrupt changes [75]. In relation to the $PM_{2.5}$ concentrations, the results showed AR terms between 0 and 1 during the E2.1 strict isolation scenario. In the short term, the AR terms varied between 0 and 11. The results suggested that, in the short term, strict isolation measures tended to reduce the persistence over time of the $PM_{2.5}$ concentrations. Thus, it was suggested that, in the short term, strict isolation measures generated a greater reduction in the persistence of $PM_{2.5}$ compared to PM_{10}. This lower persistence in the finer fraction ($PM_{2.5}$) possibly decreased the toxic effects of PM on human health.

Additionally, in the long term, the results showed AR terms between 1 and 7 in the ARIMA models developed for the PM_{10} concentrations (Table 3). The results suggested that, in the long term, strict isolation measures tended to reduce the persistence over time of the PM_{10} concentrations. In relation to the $PM_{2.5}$ concentrations, in the long term, the findings showed that the AR terms varied between 0 and 1. Thus, it was suggested that, in the long term, the strict isolation measures implemented possibly did not significantly change the persistence over time of the $PM_{2.5}$ concentrations. The long-term persistence of the $PM_{2.5}$ concentrations could have been influenced by the following complex factors: regional PM transport patterns and meteorological conditions [76].

The results showed that during the E2.1 strict isolation scenario, the I term in the ARIMA models varied between 1 and 2 for the PM_{10} and $PM_{2.5}$ concentrations, respectively. In the short term (E1), a similar trend was observed for the PM_{10} and $PM_{2.5}$ concentrations (Table 3). The results suggested that the strict isolation measures implemented did not comparatively change the decreasing trend in the PM_{10} and $PM_{2.5}$ concentrations observed in the short term (Figure 2). In the long term (E3.1), the ARIMA models showed I terms = 1 and between 1 and 2 for the PM_{10} and $PM_{2.5}$ concentrations, respectively. The results suggested that, in the long term, the strict isolation measures implemented probably had a greater effect on the PM_{10} concentrations compared to the $PM_{2.5}$ concentrations. Namely, during the strict isolation scenario, a greater decreasing trend was suggested for the PM_{10} concentrations compared to the $PM_{2.5}$ concentrations.

In relation to the MA term of the ARIMA models developed during the E2.1 strict isolation scenario, the findings evidenced a variation in its magnitude between 3 and 5 and between 6 and 12 for the PM_{10} and $PM_{2.5}$ concentrations, respectively (Table 3). In the short term (E1), a variation in the MA term was observed between 1 and 7 for the PM_{10} and $PM_{2.5}$ concentrations, respectively. In general, the results suggested that, in the short term, strict isolation measures tended to increase the variations in the PM_{10} and $PM_{2.5}$ concentrations. This increase in the variation of the concentrations was greater for $PM_{2.5}$ compared to PM_{10}. The increase in the variations of the PM_{10} and $PM_{2.5}$ concentrations did not indicate an increase in the PM concentrations in the short term [77]. The variations in the concentrations in the short term were probably related to factors such as climatic effects and specific external events that were reported in the previous sections. In the long term (E3.1), a variation in the MA term was observed between 1 and 12 and between 5 and 15 for the PM_{10} and $PM_{2.5}$ concentrations, respectively. In general, the findings suggested that, in the long term, strict isolation measures (E2.1) tended to decrease the variations in the PM_{10} and $PM_{2.5}$ concentrations. It is probable that the PM concentrations were more stable and less prone to sudden peaks during this strict isolation scenario.

During the E2.2 sectorized isolation scenario, the results showed AR terms between 0 and 4 and between 0 and 1 in the ARIMA models developed for the PM_{10} and $PM_{2.5}$ concentrations, respectively. In the short term (E1), the findings showed AR terms between 2 and 6 and between 0 and 11 for the PM_{10} and $PM_{2.5}$ concentrations, respectively (Table 3). The results suggested that, in the short term, sectorized isolation measures tended to decrease the magnitude of the AR term. That is, sectorized isolation measures tended to reduce the persistence over time of the PM_{10} and $PM_{2.5}$ concentrations. It was also

suggested that, in the short term, sectorized isolation measures comparatively generated a greater reduction in the persistence of $PM_{2.5}$ compared to PM_{10}. In the long term (E3.2), the results showed AR terms between 0 and 1 and between 0 and 2 for the PM_{10} and $PM_{2.5}$ concentrations, respectively. The results suggested that, in the long term, sectorized isolation measures tended to reduce the persistence over time of the PM_{10} concentrations. In relation to the $PM_{2.5}$ concentrations, in the long term, the findings suggested that sectorized isolation measures did not considerably change their persistence over time. The long-term persistence of the $PM_{2.5}$ concentrations may have been influenced by complex factors such as regional PM transport patterns and the meteorological conditions observed [78]. The results showed that there were changes in the wind patterns during the sectorized isolation scenario, which likely influenced the dispersion and accumulation of $PM_{2.5}$. This behavior could have affected its long-term persistence. Moreover, the long-term persistence in the PM concentrations possibly depended on factors such as the duration and intensity of isolation measures, the composition of PM sources, and the subsequent economic recovery [79].

The results showed that during the E2.2 sectorized isolation scenario, the I term in the ARIMA models was equal to 2 for the PM_{10} and $PM_{2.5}$ concentrations. In the short term (E1), it was observed that the I term varied between 1 and 2 for the PM_{10} and $PM_{2.5}$ concentrations (Table 3). Comparatively, the results suggested that the sectorized isolation measures implemented did not considerably change the increasing trend in the $PM_{2.5}$ concentrations observed in the short term (Figure 2). However, with the I terms = 1 in the short term (E1) in some ARIMA models, a lesser increasing trend in the $PM_{2.5}$ concentrations was suggested during this scenario. In relation to PM_{10}, the interpretation required further analysis. Namely, in the CAR and LAF stations, an increasing trend (+) was observed, and, in the KEN and TUN stations, a decreasing trend (−) was observed in the concentrations. Therefore, the results suggested that the ARIMA models indicated with the I term the magnitude of the trend in the PM_{10} concentrations but did not indicate whether the trend was increasing (+) or decreasing (−). In the long term (E3.2), the ARIMA models showed I terms between 1 and 2 for the PM_{10} and $PM_{2.5}$ concentrations. These ARIMA findings could initially suggest that, in the long term, sectorized isolation measures possibly did not change the trend in the PM_{10} and $PM_{2.5}$ concentrations. However, in general, during the sectorized isolation scenario (E2.2), a decreasing trend (−) was observed, and, in the long term, an increasing trend (+) was observed in the PM_{10} and $PM_{2.5}$ concentrations.

In relation to the MA term of the ARIMA models for the E2.2 sectorized isolation scenario, the findings evidenced a variation between 1 and 9 and between 1 and 7 for the PM_{10} and $PM_{2.5}$ concentrations, respectively (Table 3). In the short term (E1), a variation in the MA term was observed between 1 and 7 for the PM_{10} and $PM_{2.5}$ concentrations. In general, the results suggested that, in the short term, sectorized isolation measures did not tend to considerably influence the variations in the PM_{10} and $PM_{2.5}$ concentrations. However, for the PM_{10} concentrations a slight increase in the variation of their concentrations was observed during the E2.2 sectorized isolation scenario. In the long term (E3.2), a variation in the MA term was observed between 0 and 6 and between 1 and 8 for the PM_{10} and $PM_{2.5}$ concentrations, respectively. In general, the findings suggested that, in the long term, sectorized isolation measures (E2.2) tended to slightly increase and decrease the variations in the PM_{10} and $PM_{2.5}$ concentrations, respectively. In other words, during this sectorized isolation scenario, the $PM_{2.5}$ concentrations were slightly more stable compared to the PM_{10} concentrations.

During the E2.3 flexible isolation scenario, the results showed AR terms between 0 and 8 and between 1 and 2 in the ARIMA models developed for the PM_{10} and $PM_{2.5}$ concentrations, respectively (Table 3). In the short term (E1), the findings showed AR terms between 2 and 6 and between 0 and 11 for the PM_{10} and $PM_{2.5}$ concentrations, respectively. The results suggested that, in the short term, flexible isolation measures tended to increase and decrease the magnitude of the AR term for the PM_{10} and $PM_{2.5}$ concentrations, respectively. Namely, flexible isolation measures tended to increase and reduce the persistence over time of the PM_{10} and $PM_{2.5}$ concentrations, respectively. Under

this E2.3 flexible isolation scenario, a greater difference in the persistence of the PM_{10} and $PM_{2.5}$ concentrations was hinted at. It was also suggested that, in the short term, flexible isolation measures comparatively generated a greater reduction in the persistence of $PM_{2.5}$ compared to PM_{10}. In the long term (E3.3), the results showed AR terms = 1 and between 1 and 2 for the PM_{10} and $PM_{2.5}$ concentrations, respectively. The results hinted that, in the long term, flexible isolation measures tended to increase the persistence over time of the PM_{10} concentrations. In relation to the $PM_{2.5}$ concentrations in the long term, the findings hinted that flexible isolation measures did not change their persistence over time. Indeed, the long-term persistence in the PM concentrations probably depended on factors such as the duration and intensity of isolation measures, the composition of PM sources, and the subsequent economic recovery [80].

The results showed that, during the E2.3 flexible isolation scenario, the I term in the ARIMA models was equal to 1 for the PM_{10} and $PM_{2.5}$ concentrations. In the short term (E1), it was observed that the I term varied between 1 and 2 for the PM_{10} and $PM_{2.5}$ concentrations (Table 3). Initially, the results could suggest that flexible isolation measures did not considerably change the increasing trend in the $PM_{2.5}$ concentrations observed in the short term. However, the trend observed in the PM_{10} and $PM_{2.5}$ concentrations during the E2.3 flexible isolation scenario was decreasing (Figure 2). In other words, the trends in magnitude were similar, but in the short term it was increasing (+) and during the E2.3 flexible isolation scenario it was decreasing (−). In the long term (E3.3), the ARIMA models showed I terms = 1 for the PM_{10} and $PM_{2.5}$ concentrations. These ARIMA findings suggested that, in the long term, flexible isolation measures possibly did not change the decreasing trend in the PM_{10} and $PM_{2.5}$ concentrations.

In relation to the MA term of the ARIMA models for the E2.3 flexible isolation scenario, the findings evidenced a variation between 4 and 14 and between 1 and 15 for the PM_{10} and $PM_{2.5}$ concentrations, respectively (Table 3). In the short term (E1), a variation in the MA term between 1 and 7 was observed for the PM_{10} and $PM_{2.5}$ concentrations. The results suggested that, in the short term, flexible isolation measures tended to considerably influence the variations in the PM_{10} and $PM_{2.5}$ concentrations. Namely, these flexible isolation measures possibly generated a greater variation in the PM_{10} and $PM_{2.5}$ concentrations in the short term. In the long term (E3.3), a variation in the MA term between 1 and 11 and between 1 and 8 was observed for the PM_{10} and $PM_{2.5}$ concentrations, respectively. The findings suggested that, in the long term, flexible isolation measures tended to increase the variations in the PM_{10} and $PM_{2.5}$ concentrations, respectively. This influence on the variation of the concentrations was more evident for $PM_{2.5}$ compared to PM_{10}.

4. Conclusions

The findings of this study allowed for the following conclusions to be drawn from the sequentially established COVID-19 isolation scenarios (strict, sectorized, and flexible) in the high-altitude megacity under study. This is based on the analysis of the PM concentrations using ARIMA models.

The results suggest an average order in the observed concentrations of PM_{10} and $PM_{2.5}$ according to the considered isolation scenarios (compared to the historical trend): sectorized (−28.9% and −31.7%) > strict (−29.4% and −28.3%) > flexible (−8.52% and −12.4%). The change in the sequence between the isolation scenarios is likely related to the occurrence of particular weather conditions (wind direction and precipitation) and regional PM transport episodes (forest fires and Sahara dust) during the sectorized isolation scenario. The differences in the reduction in the PM_{10} and $PM_{2.5}$ concentrations between the strict and flexible isolation scenarios were 23.8% and 12.8%, respectively.

The findings reveal that strict isolation measures have a greater effect on the simulated concentrations of PM_{10} and $PM_{2.5}$ in the short term (PM_{10}: −47.3% and $PM_{2.5}$: −54%) than in the long term (PM_{10}: −29.4% and $PM_{2.5}$: −28.3%). In the short term, these isolation measures have a greater effect on the $PM_{2.5}$ concentrations compared to the PM_{10} concen-

trations. In the long term, the effects of these strict isolation measures on the PM_{10} and $PM_{2.5}$ concentrations are similar.

The ARIMA models suggest that strict isolation measures tend to decrease the persistence over time of the PM_{10} and $PM_{2.5}$ concentrations both in the short and long term. The models also suggest that these isolation measures do not significantly modify the decreasing trend of the PM_{10} and $PM_{2.5}$ concentrations in the short term. However, in the long term, these isolation measures have a greater effect on the PM_{10} concentrations compared to the $PM_{2.5}$ concentrations, suggesting a greater downward trend of the PM_{10} concentrations. Lastly, the ARIMA models reveal that, in the short term, strict isolation measures tend to increase the variation in the PM_{10} and $PM_{2.5}$ concentrations, with a greater increase in the case of $PM_{2.5}$. Conversely, in the long term, these isolation measures tend to decrease the variations in the PM concentrations, suggesting a more stable behavior that is less prone to sudden peaks.

The ARIMA analysis suggests that flexible isolation measures tend to increase the persistence over time of the PM_{10} concentrations in the short term, while they tend to decrease the persistence of the $PM_{2.5}$ concentrations. In the long term, an increase in the persistence of the PM_{10} concentrations is suggested, while no changes in the persistence of $PM_{2.5}$ are hinted at. Lastly, the ARIMA models reveal that flexible isolation measures tend to increase the variation in the PM_{10} and $PM_{2.5}$ concentrations both in the short and long term.

Finally, this study is relevant because it highlights the effectiveness of isolation measures to reduce urban PM_{10} and $PM_{2.5}$ concentrations. Strict measures produce significant short-term reductions, while flexible measures affect the persistence of PM over time. These findings are significant for visualizing the air quality management strategies in megacities.

Author Contributions: Conceptualization, D.S.H.-M. and C.A.Z.-M.; methodology, D.S.H.-M. and C.A.Z.-M.; software, D.S.H.-M. and C.A.Z.-M.; validation, D.S.H.-M. and C.A.Z.-M.; formal analysis, D.S.H.-M., C.A.Z.-M. and H.A.R.-Q.; investigation, D.S.H.-M. and C.A.Z.-M.; resources, C.A.Z.-M. and H.A.R.-Q.; data curation, D.S.H.-M., C.A.Z.-M. and H.A.R.-Q.; writing—original draft preparation, D.S.H.-M.; writing—review and editing, C.A.Z.-M. and H.A.R.-Q.; visualization, D.S.H.-M., C.A.Z.-M. and H.A.R.-Q.; supervision, C.A.Z.-M.; project administration, C.A.Z.-M.; funding acquisition, C.A.Z.-M. and H.A.R.-Q. All authors have read and agreed to the published version of the manuscript.

Funding: This research received no external funding.

Institutional Review Board Statement: Not applicable.

Informed Consent Statement: Not applicable.

Data Availability Statement: The data presented in this study are available on request from the corresponding author. The data are not publicly available due to privacy.

Acknowledgments: The authors wish to acknowledge the support provided by the Environmental Engineering Research Group (GIIAUD) of the Universidad Distrital Francisco José de Caldas (Colombia).

Conflicts of Interest: The authors declare no conflict of interest.

References

1. World Health Organization (WHO). *WHO Global Air Quality Guidelines*; World Health Organization: Geneva, Switzerland, 2021; ISBN 978-92-4-003422-8.
2. World Health Organization (WHO). Air Pollution. In *Compendium of WHO and Other UN Guidance on Health and Environment, 2022 Update*; (WHO/HEP/ECH/EHD/22.01); WHO: Geneva, Switzerland, 2022; Volume 2019.
3. Instituto de Hidrología. Meteorología y Estudios Ambientales (IDEAM) Contaminantes del Aire y Sus Efectos. In *Gestión de la Calidad del aire en las Ciudades de America Latina*; Banco Mundial, Ed.; Banco Mundial: Bogotá, Colombia, 2002; pp. 15–57.
4. Liou, Y.A.; Vo, T.H.; Nguyen, K.A.; Terry, J.P. Air Quality Improvement Following COVID-19 Lockdown Measures and Projected Benefits for Environmental Health. *Remote Sens.* **2023**, *15*, 530. [CrossRef]

5. Chauhan, B.V.S.; Corada, K.; Young, C.; Smallbone, K.L.; Wyche, K.P. Review on Sampling Methods and Health Impacts of Fine (PM2.5, ≤2.5 Mm) and Ultrafine (UFP, PM0.1, ≤0.1 Mm) Particles. *Atmosphere* **2024**, *15*, 572. [CrossRef]
6. Hao, Y.; Meng, X.; Yu, X.; Lei, M.; Li, W.; Yang, W.; Shi, F.; Xie, S. Quantification of Primary and Secondary Sources to PM2.5 Using an Improved Source Regional Apportionment Method in an Industrial City, China. *Sci. Total Environ.* **2020**, *706*, 135715. [CrossRef] [PubMed]
7. Mendez-Espinosa, J.F.; Rojas, N.Y.; Vargas, J.; Pachón, J.E.; Belalcazar, L.C.; Ramírez, O. Air Quality Variations in Northern South America during the COVID-19 Lockdown. *Sci. Total Environ.* **2020**, *749*, 141621. [CrossRef]
8. Zheng, S.; Fu, Y.; Sun, Y.; Zhang, C.; Wang, Y.; Lichtfouse, E. High Resolution Mapping of Nighttime Light and Air Pollutants during the COVID-19 Lockdown in Wuhan. *Environ. Chem. Lett.* **2021**, *1*, 3. [CrossRef] [PubMed]
9. Kutralam-Muniasamy, G.; Pérez-Guevara, F.; Roy, P.D.; Elizalde-Martínez, I.; Shruti, V.C. Impacts of the COVID-19 Lockdown on Air Quality and Its Association with Human Mortality Trends in Megapolis Mexico City. *Air Qual. Atmos. Health* **2021**, *14*, 553–562. [CrossRef] [PubMed]
10. Mashayekhi, R.; Pavlovic, R.; Racine, J.; Moran, M.D.; Manseau, P.M.; Duhamel, A.; Katal, A.; Miville, J.; Niemi, D.; Peng, S.J.; et al. Isolating the Impact of COVID-19 Lockdown Measures on Urban Air Quality in Canada. *Air Qual. Atmos. Health* **2021**, *14*, 1549–1570. [CrossRef]
11. Rogulski, M.; Badyda, A. Air Pollution Observations in Selected Locations in Poland during the Lockdown Related to COVID-19. *Atmosphere* **2021**, *12*, 806. [CrossRef]
12. Vega, E.; Namdeo, A.; Bramwell, L.; Miquelajauregui, Y.; Resendiz-Martinez, C.G.; Jaimes-Palomera, M.; Luna-Falfan, F.; Terrazas-Ahumada, A.; Maji, K.J.; Entwistle, J.; et al. Changes in Air Quality in Mexico City, London and Delhi in Response to Various Stages and Levels of Lockdowns and Easing of Restrictions during COVID-19 Pandemic. *Environ. Pollut.* **2021**, *285*, 117664. [CrossRef]
13. Polednik, B. Air Quality Changes in a Central European City during COVID-19 Lockdown. *Sustain. Cities Soc.* **2021**, *73*, 103096. [CrossRef]
14. Toro, A.R.; Catalán, F.; Urdanivia, F.R.; Rojas, J.P.; Manzano, C.A.; Seguel, R.; Gallardo, L.; Osses, M.; Pantoja, N.; Leiva-Guzman, M.A. Air Pollution and COVID-19 Lockdown in a Large South American City: Santiago Metropolitan Area, Chile. *Urban Clim.* **2021**, *36*, 100803. [CrossRef] [PubMed]
15. Munir, S.; Coskuner, G.; Jassim, M.S.; Aina, Y.A.; Ali, A.; Mayfield, M. Changes in Air Quality Associated with Mobility Trends and Meteorological Conditions during COVID-19 Lockdown in Northern England, UK. *Atmosphere* **2021**, *12*, 504. [CrossRef]
16. Xin, Y.; Shao, S.; Wang, Z.; Xu, Z.; Li, H. COVID-2019 Lockdown in Beijing: A Rare Opportunity to Analyze the Contribution Rate of Road Traffic to Air Pollutants. *Sustain. Cities Soc.* **2021**, *285*, 102989. [CrossRef]
17. Aljahdali, M.O.; Alhassan, A.B.; Albeladi, M.N. Impact of Novel Coronavirus Disease (COVID-19) Lockdown on Ambient Air Quality of Saudi Arabia. *Saudi J. Biol. Sci.* **2021**, *28*, 1356–1364. [CrossRef] [PubMed]
18. Teixidó, O.; Tobías, A.; Massagué, J.; Mohamed, R.; Ekaabi, R.; Hamed, H.I.; Perry, R.; Querol, X.; Al Hosani, S. The Influence of COVID-19 Preventive Measures on the Air Quality in Abu Dhabi (United Arab Emirates). *Air Qual. Atmos. Health* **2021**, *14*, 1071–1079. [CrossRef] [PubMed]
19. Sbai, S.E.; Mejjad, N.; Norelyaqine, A.; Bentayeb, F. Air Quality Change during the COVID-19 Pandemic Lockdown over the Auvergne-Rhône-Alpes Region, France. *Air Qual. Atmos. Health* **2021**, *14*, 617–628. [CrossRef] [PubMed]
20. Kolluru, S.S.R.; Patra, A.K.; Nazneen; Shiva Nagendra, S.M. Association of Air Pollution and Meteorological Variables with COVID-19 Incidence: Evidence from Five Megacities in India. *Environ. Res.* **2021**, *195*, 110854. [CrossRef] [PubMed]
21. Arregocés, H.A.; Rojano, R.; Restrepo, G. Impact of Lockdown on Particulate Matter Concentrations in Colombia during the COVID-19 Pandemic. *Sci. Total Environ.* **2021**, *764*, 142874. [CrossRef] [PubMed]
22. Zárate, E.; Carlos Belalcázar, L.; Clappier, A.; Manzi, V.; Van den Bergh, H. Air Quality Modelling over Bogota, Colombia: Combined Techniques to Estimate and Evaluate Emission Inventories. *Atmos. Environ.* **2007**, *41*, 6302–6318. [CrossRef]
23. Secretaría Distrital de Ambiente (SDA). *Informe Anual de Calidad del Aire Año 2020*; SDA: Bogotá, Colombia, 2021.
24. Secretaría Distrital de Ambiente (SDA). *Informe Anual de Calidad del Aire Año 2021*; SDA: Bogotá, Colombia, 2022.
25. Secretaría Distrital de Ambiente (SDA). *Informe Anual de Calidad del Aire Año 2019*; SDA: Bogotá, Colombia, 2020.
26. Cheng, Y.; Zhang, H.; Liu, Z.; Chen, L.; Wang, P. Hybrid Algorithm for Short-Term Forecasting of PM2.5 in China. *Atmos. Environ.* **2019**, *200*, 264–279. [CrossRef]
27. García Nieto, P.J.; Sánchez Lasheras, F.; García-Gonzalo, E.; de Cos Juez, F.J. PM10 Concentration Forecasting in the Metropolitan Area of Oviedo (Northern Spain) Using Models Based on SVM, MLP, VARMA and ARIMA: A Case Study. *Sci. Total Environ.* **2018**, *621*, 753–761. [CrossRef] [PubMed]
28. He, J.; Zhang, Y.; Wang, K.; Chen, Y.; Leung, L.R.; Fan, J.; Li, M.; Zheng, B.; Zhang, Q.; Duan, F.; et al. Multi-Year Application of WRF-CAM5 over East Asia-Part I: Comprehensive Evaluation and Formation Regimes of O3 and PM 2.5. *Atmos. Environ.* **2017**, *165*, 122–142. [CrossRef]
29. Song, C.; Fu, X. Research on Different Weight Combination in Air Quality Forecasting Models. *J. Clean. Prod.* **2020**, *261*, 121169. [CrossRef]
30. Jamil, R. Hydroelectricity Consumption Forecast for Pakistan Using ARIMA Modeling and Supply-Demand Analysis for the Year 2030. *Renew. Energy* **2020**, *154*, 1–10. [CrossRef]

31. Zhang, L.; Lin, J.; Qiu, R.; Hu, X.; Zhang, H.; Chen, Q.; Tan, H.; Lin, D.; Wang, J. Trend Analysis and Forecast of PM2.5 in Fuzhou, China Using the ARIMA Model. *Ecol. Indic.* **2018**, *95*, 702–710. [CrossRef]
32. Allende, H.; Moraga, C.; Salas, R. Artificial Neural Networks in Time Series Forecasting: A Comparative Analysis. *Kybernetika* **2002**, *38*, 685–707.
33. Guerrero Guzmán, V.M. *Análisis Estadístico de Series de Tiempo Económicas*, 2nd ed.; Thomson Editores, S.A., Ed.; UNAM: Ciudad de México, Mexico, 2003; ISBN 970-686-326-5.
34. Díaz-Robles, L.A.; Ortega, J.C.; Fu, J.S.; Reed, G.D.; Chow, J.C.; Watson, J.G.; Moncada-Herrera, J.A. A Hybrid ARIMA and Artificial Neural Networks Model to Forecast Particulate Matter in Urban Areas: The Case of Temuco, Chile. *Atmos. Environ.* **2008**, *42*, 8331–8340. [CrossRef]
35. Das, R.; Middya, A.I.; Roy, S. High Granular and Short Term Time Series Forecasting of $PM_{2.5}$ Air Pollutant—A Comparative Review. *Artif. Intell. Rev.* **2021**, *55*, 1253–1287. [CrossRef]
36. Cekim, H.O. Forecasting PM10 Concentrations Using Time Series Models: A Case of the Most Polluted Cities in Turkey. *Environ. Sci. Pollut. Res.* **2020**, *27*, 25612–25624. [CrossRef]
37. Photphanloet, C.; Lipikorn, R. PM10 Concentration Forecast Using Modified Depth-First Search and Supervised Learning Neural Network. *Sci. Total Environ.* **2020**, *727*, 138507. [CrossRef]
38. Grivas, G.; Chaloulakou, A. Artificial Neural Network Models for Prediction of PM10 Hourly Concentrations, in the Greater Area of Athens, Greece. *Atmos. Environ.* **2006**, *40*, 1216–1229. [CrossRef]
39. Taneja, K.; Ahmad, S.; Ahmad, K.; Attri, S.D. Time Series Analysis of Aerosol Optical Depth over New Delhi Using Box–Jenkins ARIMA Modeling Approach. *Atmos. Pollut. Res.* **2016**, *7*, 585–596. [CrossRef]
40. Zafra, C.; Ángel, Y.; Torres, E. ARIMA Analysis of the Effect of Land Surface Coverage on PM10 Concentrations in a High-Altitude Megacity. *Atmos. Pollut. Res.* **2017**, *8*, 660–668. [CrossRef]
41. Zukaib, U.; Maray, M.; Mustafa, S.; Haq, N.U.; Khan, A.R.; Rehman, F. Impact of COVID-19 Lockdown on Air Quality Analyzed through Machine Learning Techniques. *PeerJ Comput. Sci.* **2023**, *9*, 1–25. [CrossRef] [PubMed]
42. Inostroza, L. Informal Urban Development in Latin American Urban Peripheries. Spatial Assessment in Bogotá, Lima and Santiago de Chile. *Landsc. Urban Plan.* **2017**, *165*, 267–279. [CrossRef]
43. Secretaría Distrital de Ambiente (SDA). *Informe Anual de Calidad del Aire Año 2016*; Alcaldía Mayor de Bogotá: Bogotá, Colombia, 2017; p. 187.
44. Hall, E.; Gilliam, J. *Reference and Equivalent Methods Used to Measure National Ambient Air Quality Standards (NAAQS) Criteria Air Pollutants—Volume I*; US Environmental Protection Agency: Washington, DC, USA, 2016.
45. Compendium of Methods for the Determination of Inorganic Compounds in Ambient Air. *United States Enviromental Protection Agency (US. EPA). List of Designated Reference and Equivalent Methods*; EPA: Cincinatty, OH, USA, 2018; p. 72.
46. Chehrassan, M.; Nikouei, F.; Shakeri, M.; Behnamnia, A.; Mahabadi, E.A.; Ghandhari, H. The Role of Environmental and Seasonal Factors in Spine Deep Surgical Site Infection: The Air Pollution, a Factor That May Be Underestimated. *Eur. Spine J.* **2024**, *33*, 1–6. [CrossRef] [PubMed]
47. Urbanowicz, T.; Skotak, K.; Olasińska-Wiśniewska, A.; Filipiak, K.J.; Bratkowski, J.; Wyrwa, M.; Sikora, J.; Tyburski, P.; Krasińska, B.; Krasiński, Z.; et al. Long-Term Exposure to PM10 Air Pollution Exaggerates Progression of Coronary Artery Disease. *Atmosphere* **2024**, *15*, 216. [CrossRef]
48. Kotsiou, O.S.; Saharidis, G.K.D.; Kalantzis, G.; Fradelos, E.C.; Gourgoulianis, K.I. The Impact of the Lockdown Caused by the COVID-19 Pandemic on the Fine Particulate Matter (PM2.5) Air Pollution: The Greek Paradigm. *Int. J. Environ. Res. Public Health* **2021**, *18*, 6748. [CrossRef] [PubMed]
49. Alsaber, A.R.; Pan, J.; Al-Hurban, A. Handling Complex Missing Data Using Random Forest Approach for an Air Quality Monitoring Dataset: A Case Study of Kuwait Environmental Data (2012 to 2018). *Int. J. Environ. Res. Public Health* **2021**, *18*, 1333. [CrossRef]
50. Kim, T.; Kim, J.; Yang, W.; Lee, H.; Choo, J. Missing Value Imputation of Time-Series Air-Quality Data via Deep Neural Networks. *Int. J. Environ. Res. Public Health* **2021**, *18*, 12213. [CrossRef]
51. Van Buuren, S.; Groothuis-Oudshoorn, K. Mice: Multivariate Imputation by Chained Equations in R. *J. Stat. Softw.* **2011**, *45*, 1–67. [CrossRef]
52. Stekhoven, D.J.; Bühlmann, P. Missforest-Non-Parametric Missing Value Imputation for Mixed-Type Data. *Bioinformatics* **2012**, *28*, 112–118. [CrossRef] [PubMed]
53. Box, G.; Jenkins, G. *Times Series Analysis: Forecasting and Control*, 2nd ed.; Holden Day, Ed.; Holden Day: San Fransico, CA, USA, 1970; ISBN 0-8162-1104-3.
54. Zafra-Mejía, C.A.; Rondón-Quintana, H.A.; Urazán-Bonells, C.F. ARIMA and TFARIMA Analysis of the Main Water Quality Parameters in the Initial Components of a Megacity's Drinking Water Supply System. *Hydrology* **2024**, *11*, 10. [CrossRef]
55. Zheleva, I.; Veleva, E.; Filipova, M. Analysis and Modeling of Daily Air Pollutants in the City of Ruse, Bulgaria. *AIP Conf. Proc.* **2017**, *1895*, 030007. [CrossRef]
56. Zafra-Mejía, C.A.; Zuluaga-Astudillo, D.A.; Rondón-Quintana, H.A. Analysis of the Landfill Leachate Treatment System Using Arima Models: A Case Study in a Megacity. *Appl. Sci.* **2021**, *11*, 6988. [CrossRef]
57. Castells-Quintana, D.; Herrera-Idárraga, P.; Quintero, L.E.; Sinisterra, G. Unequal Response to Mobility Restrictions: Evidence from COVID-19 Lockdown in the City of Bogotá. *Spat. Econ. Anal.* **2023**, *18*, 1–19. [CrossRef]

58. Caicedo, J.D.; Walker, J.L.; González, M.C. Influence of Socioeconomic Factors on Transit Demand During the COVID-19 Pandemic: A Case Study of Bogotá's BRT System. *Front. Built Environ.* **2021**, *7*, 1–15. [CrossRef]
59. Blackman, A.; Bonilla, J.A.; Villalobos, L. Quantifying COVID-19's Silver Lining: Avoided Deaths from Air Quality Improvements in Bogotá. *J. Environ. Econ. Manag.* **2023**, *117*, 102749. [CrossRef]
60. Vallejo-Borda, J.A.; Giesen, R.; Basnak, P.; Reyes, J.P.; Mella Lira, B.; Beck, M.J.; Hensher, D.A.; de Dios Ortúzar, J. Characterising Public Transport Shifting to Active and Private Modes in South American Capitals during the COVID-19 Pandemic. *Transp. Res. Part A Policy Pract.* **2022**, *164*, 186–205. [CrossRef]
61. Sulaymon, I.D.; Zhang, Y.; Hopke, P.K.; Zhang, Y.; Hua, J.; Mei, X. COVID-19 Pandemic in Wuhan: Ambient Air Quality and the Relationships between Criteria Air Pollutants and Meteorological Variables before, during, and after Lockdown. *Atmos. Res.* **2021**, *250*, 105362. [CrossRef]
62. Shahriar, S.A.; Kayes, I.; Hasan, K.; Hasan, M.; Islam, R.; Awang, N.R.; Hamzah, Z.; Rak, A.E.; Salam, M.A. Potential of Arima-Ann, Arima-Svm, Dt and Catboost for Atmospheric Pm2.5 Forecasting in Bangladesh. *Atmosphere* **2021**, *12*, 100. [CrossRef]
63. Collado, C.F.; Lucio, P.B. *Metodología de la Investigación*; Mcgraw-Hill: Ciudad de México, Mexico, 2014; ISBN 978-1-4562-2396-0.
64. Shi, Z.; Song, C.; Liu, B.; Lu, G.; Xu, J.; Vu, T.V.; Elliott, R.J.R.; Li, W.; Bloss, W.J.; Harrison, R.M. Abrupt but Smaller than Expected Changes in Surface Air Quality Attributable to COVID-19 Lockdowns. *Sci. Adv.* **2021**, *7*, eabd6696. [CrossRef] [PubMed]
65. Nidzgorska-Lencewicz, J. Application of Artificial Neural Networks in the Prediction of PM10 Levels in the Winter Months: A Case Study in the Tricity Agglomeration, Poland. *Atmosphere* **2018**, *9*, 203. [CrossRef]
66. Borhani, F.; Shafiepour Motlagh, M.; Stohl, A.; Rashidi, Y.; Ehsani, A.H. Changes in Short-Lived Climate Pollutants during the COVID-19 Pandemic in Tehran, Iran. *Environ. Monit. Assess.* **2021**, *193*, 331. [CrossRef] [PubMed]
67. Gao, C.; Li, S.; Liu, M.; Zhang, F.; Achal, V.; Tu, Y.; Zhang, S.; Cai, C. Impact of the COVID-19 Pandemic on Air Pollution in Chinese Megacities from the Perspective of Traffic Volume and Meteorological Factors. *Sci. Total Environ.* **2021**, *773*, 145545. [CrossRef]
68. El-Sayed, M.M.H.; Elshorbany, Y.F.; Koehler, K. On the Impact of the COVID-19 Pandemic on Air Quality in Florida. *Environ. Pollut.* **2021**, *285*, 117451. [CrossRef] [PubMed]
69. Brandao, R.; Foroutan, H. Air Quality in Southeast Brazil during COVID-19 Lockdown: A Combined Satellite and Ground-Based Data Analysis. *Atmosphere* **2021**, *12*, 583. [CrossRef]
70. Rudke, A.P.; Martins, J.A.; de Almeida, D.S.; Martins, L.D.; Beal, A.; Hallak, R.; Freitas, E.D.; Andrade, M.F.; Foroutan, H.; Baek, B.H.; et al. How Mobility Restrictions Policy and Atmospheric Conditions Impacted Air Quality in the State of São Paulo during the COVID-19 Outbreak. *Environ. Res.* **2021**, *198*, 111255. [CrossRef]
71. Vlachogianni, A.; Kassomenos, P.; Karppinen, A.; Karakitsios, S.; Kukkonen, J. Evaluation of a Multiple Regression Model for the Forecasting of the Concentrations of NOx and PM10 in Athens and Helsinki. *Sci. Total Environ.* **2011**, *409*, 1559–1571. [CrossRef]
72. Franceschi, F.; Cobo, M.; Figueredo, M. Discovering Relationships and Forecasting PM10 and PM2.5 Concentrations in Bogotá, Colombia, Using Artificial Neural Networks, Principal Component Analysis, and k-Means Clustering. *Atmos. Pollut. Res.* **2018**, *9*, 912–922. [CrossRef]
73. Sulaymon, I.D.; Zhang, Y.; Hopke, P.K.; Hu, J.; Zhang, Y.; Li, L.; Mei, X.; Gong, K.; Shi, Z.; Zhao, B.; et al. Persistent High PM2.5 Pollution Driven by Unfavorable Meteorological Conditions during the COVID-19 Lockdown Period in the Beijing-Tianjin-Hebei Region, China. *Environ. Res.* **2021**, *198*, 111186. [CrossRef]
74. Rojas, J.P.; Urdanivia, F.R.; Garay, R.A.; García, A.J.; Enciso, C.; Medina, E.A.; Toro, R.A.; Manzano, C.; Leiva-Guzmán, M.A. Effects of COVID-19 Pandemic Control Measures on Air Pollution in Lima Metropolitan Area, Peru in South America. *Air Qual. Atmos. Health* **2021**, *14*, 925–933. [CrossRef] [PubMed]
75. Jian, L.; Zhao, Y.; Zhu, Y.-P.; Zhang, M.-B.; Bertolatti, D. An Application of ARIMA Model to Predict Submicron Particle Concentrations from Meteorological Factors at a Busy Roadside in Hangzhou, China. *Sci. Total Environ.* **2012**, *426*, 336–345. [CrossRef] [PubMed]
76. Silva, A.C.T.; Branco, P.T.B.S.; Sousa, S.I.V. Impact of COVID-19 Pandemic on Air Quality: A Systematic Review. *Int. J. Environ. Res. Public Health* **2022**, *19*, 1950. [CrossRef] [PubMed]
77. Islam, M.S.; Chowdhury, T.A. Effect of COVID-19 Pandemic-Induced Lockdown (General Holiday) on Air Quality of Dhaka City. *Environ. Monit. Assess.* **2021**, *193*, 343. [CrossRef] [PubMed]
78. Adam, M.G.; Tran, P.T.M.; Balasubramanian, R. Air Quality Changes in Cities during the COVID-19 Lockdown: A Critical Review. *Atmos. Res.* **2021**, *264*, 105823. [CrossRef] [PubMed]
79. Hassan, M.A.; Mehmood, T.; Lodhi, E.; Bilal, M.; Dar, A.A.; Liu, J. Lockdown Amid COVID-19 Ascendancy over Ambient Particulate Matter Pollution Anomaly. *Int. J. Environ. Res. Public Health* **2022**, *19*, 13540. [CrossRef]
80. Brodeur, A.; Gray, D.; Islam, A.; Bhuiyan, S. A Literature Review of the Economics of COVID-19. *J. Econ. Surv.* **2021**, *35*, 1007–1044. [CrossRef]